ISSN 1674-1056
http://cpb.iphy.ac.cn
http://iopscience.iop.org/cpb
中国物理 B
Chinese Physics
中国物理 Chinese Physics B

Responsivity and noise characteristics of AlGaN/GaN-HEMT terahertz detectors at elevated temperatures

Zhi-Feng Tian(田志锋), Peng Xu(徐鹏), Yao Yu(余耀), Jian-Dong Sun(孙建东), Wei Feng(冯伟), Qing-Feng Ding(丁青峰), Zhan-Wei Meng(孟占伟), Xiang Li(李想), Jin-Hua Cai(蔡金华), Zhong-Xin Zheng(郑中信), Xin-Xing Li(李欣幸), Lin Jin(靳琳), Hua Qin(秦华), Yun-Fei Sun(孙云飞)

Citation: Chin. Phys. B . 2019, 28(5): 058501. **doi:** 10.1088/1674-1056/28/5/058501
Journal homepage: http://cpb.iphy.ac.cn; http://iopscience.iop.org/cpb

What follows is a list of articles you may be interested in

Metal halide perovskite photodetectors: Material featuresand device engineering

Ye Wang(王烨), Meng-Lei Gao(高孟磊), Jin-Liang Wu(吴金良), Xing-Wang Zhang(张兴旺)
Chin. Phys. B . 2019, 28(1): 018502. **doi:** 10.1088/1674-1056/28/1/018502

Improved carrier injection and confinement in InGaN light-emitting diodes containing GaN/AlGaN/GaN triangular barriers

Li-Wen Cheng(程立文), Jian Ma(马剑), Chang-Rui Cao(曹常锐), Zuo-Zheng Xu(徐作政), Tian Lan(兰天), Jin-Peng Yang(杨金彭), Hai-Tao Chen(陈海涛), Hong-Yan Yu(于洪岩), Shu-Dong Wu(吴曙东), Shun Yao(尧舜), Xiang-Hua Zeng(曾祥华), Zai-Quan Xu(徐仔全)
Chin. Phys. B . 2018, 27(8): 088504. **doi:** 10.1088/1674-1056/27/8/088504

Fabrication and characterization of novel high-speed InGaAs/InP uni-traveling-carrier photodetector for high responsivity

Chen Qing-Tao, Huang Yong-Qing, Fei Jia-Rui, Duan Xiao-Feng, Liu Kai, Liu Feng, Kang Chao, Wang Jun-Chu, Fang Wen-Jing, Ren Xiao-Min
Chin. Phys. B . 2015, 24(10): 108506. **doi:** 10.1088/1674-1056/24/10/108506

Analysis on high speed response of a uni-traveling-carrier double hetero-junction phototransistor

Jiang Zhi-Yun, Xie Hong-Yun, Zhang Liang-Hao, Zhang Wan-Rong, Hu Rui-Xin, Huo Wen-Juan
Chin. Phys. B . 2015, 24(4): 048504. **doi:** 10.1088/1674-1056/24/4/048504

Enhanced near-infrared responsivity of silicon photodetector by the impurity photovoltaic effect

Yuan Ji-Ren, Huang Hai-Bin, Deng Xin-Hua, Liang Xiao-Jun, Zhou Nai-Gen, Zhou Lang
Chin. Phys. B . 2015, 24(4): 048501. **doi:** 10.1088/1674-1056/24/4/048501

Responsivity and noise characteristics of AlGaN/GaN-HEMT terahertz detectors at elevated temperatures*

Zhi-Feng Tian(田志锋)[1,2,3,5], Peng Xu(徐鹏)[1,4], Yao Yu(余耀)[1,5], Jian-Dong Sun(孙建东)[1,†], Wei Feng(冯伟)[1,6], Qing-Feng Ding(丁青峰)[1,2], Zhan-Wei Meng(孟占伟)[1,4], Xiang Li(李想)[1,6], Jin-Hua Cai(蔡金华)[1], Zhong-Xin Zheng(郑中信)[7], Xin-Xing Li(李欣幸)[1], Lin Jin(靳琳)[1], Hua Qin(秦华)[1,2,5,‡], and Yun-Fei Sun(孙云飞)[8]

[1] *Key Laboratory of Nano Devices and Applications, Suzhou Institute of Nano-tech and Nano-bionics, Chinese Academy of Sciences, Suzhou* 215123, *China*
[2] *School of Physical Science and Technology, ShanghaiTech University, Shanghai* 200000, *China*
[3] *Shanghai Institute of Ceramics, Chinese Academy of Sciences, Shanghai* 200000, *China*
[4] *Nano Science and Technology Institute, University of Science and Technology of China, Hefei* 230026, *China*
[5] *University of Chinese Academy of Sciences, Beijing* 100049, *China*
[6] *School of Nano Technology and Nano Bionics, University of Science and Technology of China, Hefei* 230026, *China*
[7] *Beijing Huahang Radio Measurement & Research Institute, Beijing* 100013, *China*
[8] *College of Electronic and Information Engineering, Suzhou University of Sciences and Technology, Suzhou* 215009, *China*

(Received 17 January 2019; revised manuscript received 27 February 2019; published online 4 April 2019)

The responsivity and the noise of a detector determine the sensitivity. Thermal energy usually affects both the responsivity and the noise spectral density. In this work, the noise characteristics and responsivity of an antenna-coupled AlGaN/GaN high-electron-mobility-transistor (HEMT) terahertz detector are evaluated at temperatures elevated from 300 K to 473 K. Noise spectrum measurement and a simultaneous measurement of the source–drain conductance and the terahertz photocurrent allow for detailed analysis of the electrical characteristics, the photoresponse, and the noise behavior. The responsivity is reduced from 59 mA/W to 11 mA/W by increasing the detector temperature from 300 K to 473 K. However, the noise spectral density maintains rather constantly around 1–2 $\mathrm{pA/Hz^{1/2}}$ at temperatures below 448 K, above which the noise spectrum abruptly shifts from Johnson-noise type into flicker-noise type and the noise density is increased up to one order of magnitude. The noise-equivalent power (NEP) is increased from 22 $\mathrm{pW/Hz^{1/2}}$ at 300 K to 60 $\mathrm{pW/Hz^{1/2}}$ at 448 K mainly due to the reduction in mobility. Above 448 K, the NEP is increased up to 1000 $\mathrm{pW/Hz^{1/2}}$ due to the strongly enhanced noise. The sensitivity can be recovered by cooling the detector back to room temperature.

Keywords: terahertz detection, gallium nitride, noise spectrum, responsivity

PACS: 85.60.Gz, 72.80.Ey, 81.40.Gh, 87.50.U– **DOI:** 10.1088/1674-1056/28/5/058501

1. Introduction

Terahertz electromagnetic wave spectra contain broad information in physics, chemistry, and material construction. Terahertz science and technology have made remarkable progress in various applications, such as space detection, biomedical diagnosis, security screening, and communication.[1–5] A terahertz application system always contains at least one emitter–detector chain. The figure-of-merit of the emitter–detector chain affects the performance of the system. Hence, the terahertz source and detector implemented in the chain are the two most important devices as the physical base of the system. Once the emitter power is fixed, the detector sensitivity becomes the key factor affecting the signal-to-noise ratio. The detector sensitivity is guaranteed not only by the detection mechanism, but also by the device design and the characteristics of the electronic material implemented. In terahertz applications, detectors may be placed in harsh environments, for example at temperatures higher than the ambient temperature. For high-sensitivity terahertz detectors, one of the limiting factors is the detector noise which is usually dominated by the thermal noise,[6] shot noise,[7] flicker noise,[8–10] etc. The lower the noise is, the higher the sensitivity that could be achieved. Understanding the noise characteristics of a terahertz detector at elevated temperatures is essential for enhancing the sensitivity. Previously, Hou *et al.*[11] reported GaN-based terahertz detectors operated at 0.14 THz based on Seebeck effect by elevating the temperature. They showed the advantages of the detectors at high temperature and the analysis of physical mechanism responsible for the temperature dependence of responsivity and noise-equivalent power (NEP). However, more details on the electron density, mobility, threshold voltage, and connection between sensitivity and responsivity and noise characteristics were not discussed. In our previous work,[12] antenna-coupled

*Project supported by the National Key Research and Development Program of China (Grant No. 2016YFF0100501), the National Natural Science Foundation of China (Grant Nos. 61771466, 61775231, and 61611530708), the Six Talent Peaks Project of Jiangsu Province, China (Grant No. XXRJ-079), and the Youth Innovation Promotion Association of Chinese Academy of Sciences (Grant No. 2017372).

†Corresponding author. E-mail: jdsun2008@sinano.ac.cn
‡Corresponding author. E-mail: hqin2007@sinano.ac.cn

© 2019 Chinese Physical Society and IOP Publishing Ltd

AlGaN/GaN high-electron-mobility-transistor (HEMT) detectors operated at 0.34 THz, 0.65 THz, and 0.90 THz offered increased sensitivities due to the enhanced responsivity and reduced noise at 77 K, allowing for sensing of incoherent blackbody emission. Here, in this work we report the reduction in sensitivity of a similar detector designed for 0.34 THz based on self-mixing mechanism by elevating the detector temperature from 300 K to 473 K. The temperature-dependent mobility, responsivity, and noise spectrum are characterized to reveal the corresponding contributions to the sensitivity reduction.

2. Device model and experiment setup

By using a similar detector design based on AlGaN/GaN two-dimensional-electron-gas (2DEG), and a fabrication process reported in Ref. [13], the antenna-coupled AlGaN/GaN-HEMT detector has a center response frequency around 0.34 THz and partial views of the optical micrograph can be seen in our previous work.[12] As schematically shown in Fig. 1(a), the detector is operated with a proper gate voltage ($V_{\rm G}$) as a self-mixing device which converts the incident terahertz power with the electrical polarization along the channel into a direct-current photocurrent (i_0) flowing from the source to the drain. When the photocurrent ($i_{\rm T}$) is read out by a current preamplifier, the detector can be modeled as a short-circuited current source with internal impedance $R_{\rm ch} = 1/G_0 = L/W\mu C_{\rm G}(V_{\rm G} - V_{\rm TH})$ and series resistance $2r_1$, as shown in Fig. 1(b), and the measured photocurrent is always less than the internal photocurrent: $i_{\rm T} = i_0/(1+2r_1G_0)$. Parameters L and W are the length and width of the channel controlled by the gate, respectively. $C_{\rm G} \approx 0.40$ μF/cm^2 is the gate-channel capacitance per unit area, μ is the electron mobility, and $V_{\rm TH}$ stands for the threshold gate voltage to deplete the channel. According to the detector model,[14–16] the external photocurrent generated with zero source–drain bias can be described as $i_{\rm T} = \Lambda \cdot \Xi \cdot P_{\rm THz}$, where antenna factor Λ counts for the conversion factor contributed by the antenna which couples the incident terahertz wave into the gated electron channel, field-effect factor $\Xi = (1-2r_1G) \times {\rm d}G/{\rm d}V_{\rm G}$ counts for the conversion factor contributed by the field-effect gate which mixes the terahertz fields and generates a DC photocurrent, and $P_{\rm THz}$ is the total terahertz power received by the detector. The responsivity (R_i) of the detector can be obtained according to $R_i = i_{\rm T}/P_{\rm THz}$. The sensitivity in terms of the noise-equivalent power is limited by the noise current ($i_{\rm n}$) seen by the current preamplifier: ${\rm NEP} = i_{\rm n}/R_i$. In our case where there is no external source–drain bias applied, the thermal noise is the dominant noise source and can be expressed as $i_{\rm n} = \sqrt{4k_{\rm B}TG}$, where T is the detector temperature.

To characterize the above detector, a measurement setup schematically shown in Fig. 1(c) is used. It is designed so that the source–drain differential conductance $G = 1/(1/G_0 + 2r_1)$ and photocurrent $i_{\rm T}$ can be measured simultaneously. The source–drain differential conductance is obtained by using lock-in amplifier #1 (Signal Recovery 7265) which outputs a small-amplitude sinusoidal signal ($V_{\rm rms} = 10$ mV, $f_{\rm ds} = 37$ Hz) and measures the output from the current preamplifier at the same frequency. By multiplying a microwave signal (9–14 GHz, 5 dBm) with a factor of 27, the terahertz source generates terahertz radiation with frequency from 0.243 THz to 0.378 THz and a power below 300 μW. By on–off (50% duty cycle) modulating the microwave signal and hence the terahertz power at $f_{\rm M} = 3177$ Hz, the photocurrent can be amplified by the same current preamplifier and then measured by lock-in amplifier #2 (Signal Recovery 7265) at $f_{\rm M} = 3177$ Hz. In order to obtain the noise spectrum from the detector in a frequency range from 200 Hz to 100 kHz, a signal analyzer (Stanford Research System 770) is used to analyze the signal from the current preamplifier.

In our experiment, the detector chip is directly attached to an insulated electrical heater. A thermoelectric couple integrated within the heater is monitored by a FLUKE 17B digital multimeter. By applying a DC voltage to the heater, the device temperature can be tuned from 300 K to 473 K. It has to be mentioned that to calibrate the responsivity of such a bare detector chip, we need to estimate the received terahertz power ($P_{\rm THz}$). The procedure is as follows.[11] The effective detector area is assumed to be $\lambda/2 \times \lambda/2$. The terahertz beam with a total power of $P_{\rm S}$ is raster scanned by the detector with a step size of $\lambda/2$ in both x and y directions. The sum of the raster scanned detector signal ($i(m,n)$) is proportional to the total power and the responsivity $\sum_{m,n} i(m,n) = R_i P_{\rm S}$. The detector location is then adjusted to the center of the beam to maximize the photocurrent which can be expressed as $i_{\rm T} = R_i P_{\rm THz}$. Hence, the received terahertz power is estimated by $P_{\rm THz} = P_{\rm S} i_{\rm T} / \sum_{m,n} i(m,n)$. Although this method is widely used for calibration purposes, large uncertainty in the estimated terahertz power exists as the detector area may differ from $\lambda^2/4$. In contrast, integration of the detector with a silicon lens allows for a direct characterization of the optical responsivity/NEP without the need to estimate the actual absorbed terahertz power. This is based on the fact that a hyperspherical silicon lens can focus the incident terahertz beam into a spot with its size close to the effective area of the antenna and the terahertz power absorbed by the detector could be maximized. Since the detector needs to be heated in our experiment, integration of the detector chip with a silicon lens may encounter unexpected problems at elevated temperatures, e.g., possible detachment of the detector chip from the silicon lens, or detachment of the silicon lens from its fixture.

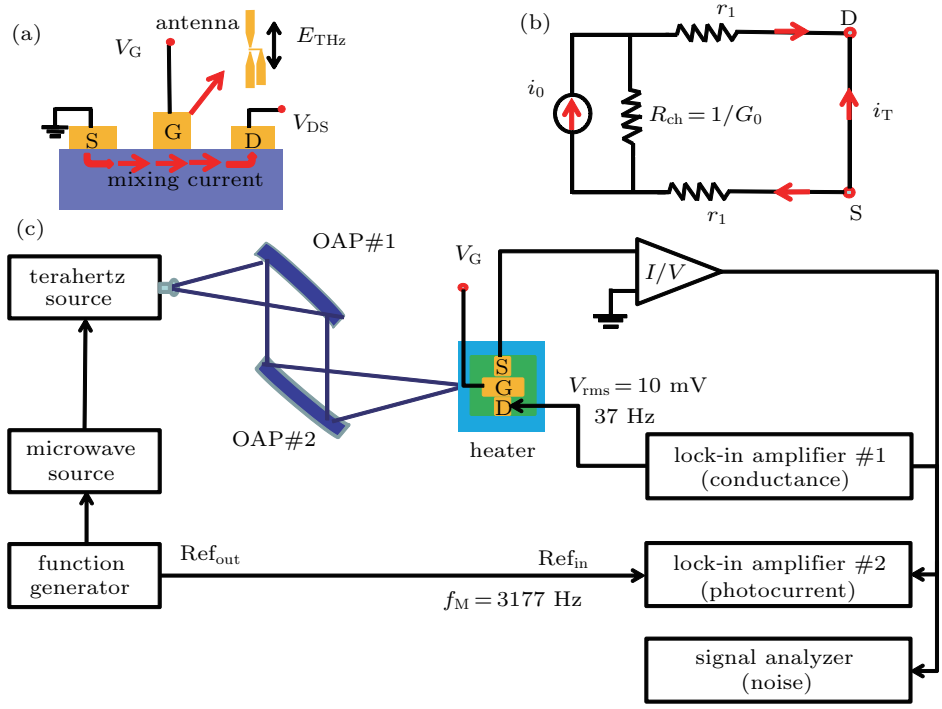


Fig. 1. (a) Device structure and (b) equivalent circuit of the AlGaN/GaN-HEMT. (c) A schematic setup for simultaneous measurement of the differential conductance and self-mixing photocurrent.

3. Results and discussion

The AlGaN/GaN-HEMT detector survived after four full thermal circles and each circle actually took about 5 h with a heating rate of 0.43–0.73 K/min from 300 K to 473 K. When the detector temperature is elevated, the source–drain conductance decreases as shown in Fig. 2(a). Along with the decrease of conductance, the threshold gate voltage is rather stable around −3.72 V except that it starts to shift to more negative gate voltages when the temperature is above 423 K, as shown in Fig. 2(b). The gate current is also monitored at different temperatures. A transition in the slope of the gate leakage current versus temperature occurs around the same temperature of 423 K. The related behaviors of the threshold voltage and leakage current infer that the electron density in the channel is fairly unchanged by the temperature below 423 K.[17,18] In contrast, the electron mobility decreases with a $T^{-3/2}$ dependence for phonon dominated scattering,[19] which leads to the result that the conductance is more sensitive to changes of temperature. The inset of Fig. 2(a) shows the temperature-dependent conductance with a zero gate voltage and it can be fitted well with an exponential curve $G = 2.22\exp[-T/(376.97-273.15)] + 0.02$ [mS]. As we will show in the following, the change in conductance is mainly caused by the degradation in electron mobility.

According to the self-mixing model, the photocurrent as a function of the gate voltage is proportional to the field-effect factor. This characteristic is well confirmed by comparing the photocurrent data obtained at various temperatures shown in Fig. 2(c) with the conductance data shown in Fig. 2(a), i.e., the maximum photocurrent always occurs at the gate voltage where field-effect factor Ξ is maximized. The maximum photocurrent has a direct connection with the magnitude of the channel conductance while the variation in the antenna factor due to the temperature change can be neglected. This is verified by examining the normalized photoresponse spectra at different temperatures. As shown in Fig. 2(d), the detector shows a stable response spectrum with a peak response around 0.33 THz which is in good agreement with the 0.34-THz-antenna design. Hence, the observed temperature dependence of photocurrent is mainly caused by the field-effect factor.

A procedure similar to that described in Ref. [14] is applied to extract channel conductance $G_0(V_G)$ and series resistance $2r_1$ from the data shown in Fig. 1(a). Since the electron density, which can be described as[21]

$$n = \frac{C_G \eta k_B T}{e^2} \ln\left[1 + \exp\left(\frac{V_G - V_{TH}}{\eta k_B T/e}\right)\right],$$

is a weak function of the temperature in the range from 300 K to 473 K. The electron density at $V_G = 0$ V can be extracted from the threshold gate voltage $n_0 = C_G V_{TH}/e$ at different temperatures. Then the electron mobility at different temperatures is estimated from the conductance at $V_G = 0$ V, i.e., $\mu = G_0(V_G = 0)L/(Wn_0e)$. As shown in Fig. 3 (a), the electron mobility decreases with the elevating temperature while the electron density is rather constant around 1×10^{13} cm^{-2}. The above procedure also gives the optimal gate voltages for the maxima of field-effect factor, i.e., the maxima of Ξ. As shown in Fig. 3(b), the extracted optimal gate voltages well agree with the measured optimal gate voltages in Fig. 2(c).

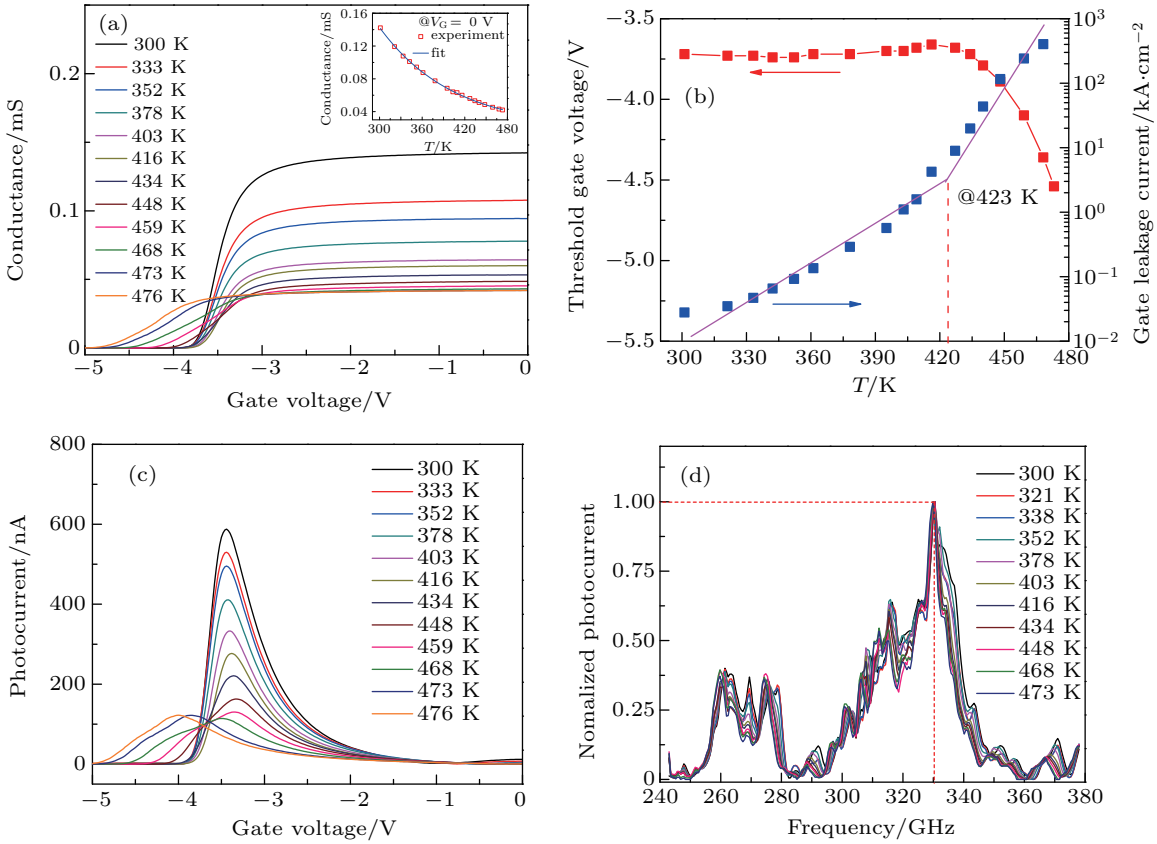


Fig. 2. (a) Measured source–drain differential conductance as a function of the gate voltage at different temperatures from 300 K to 473 K. (b) Threshold gate voltage and leakage current at $V_G = -5$ V. (c) Measured photocurrent as a function of the gate voltage. (d) Normalized self-mixing photocurrent at the optimal gate voltage as a function of the terahertz frequency.

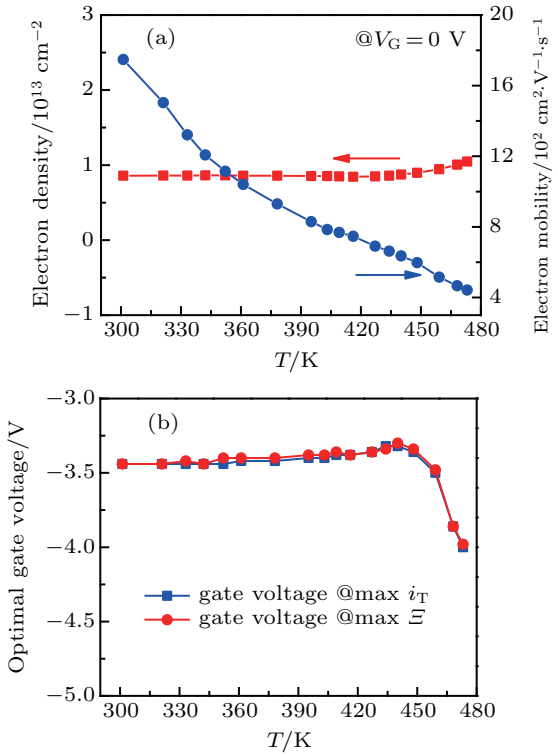


Fig. 3. (a) The extracted electron density and electron mobility as a function of temperature from 300 K to 473 K without gate bias. (b) The optimal gate voltages as a function of temperature.

From the peak photocurrent, the responsivity can be calibrated. As shown in Fig. 4(a), the responsivity decreases linearly with the temperature below 448 K, which is in accordance with the decrease in electron mobility. It is found that the responsivity decreases from 59 mA /W at 300 K to 11 mA/W at 473 K. Within the temperature range, a rise in the thermal noise could be expected. However, due to the decrease in electron mobility, i.e., an increase in the channel resistance, the overall thermal noise is kept stable around 1–2 pA/Hz$^{1/2}$ in the temperature range from 300 K to 448 K, as shown in Fig. 4(b). Detailed noise spectra at different temperatures are shown in the inset. The flicker noise can be seen with frequency below ∼1 kHz. Above 1 kHz, the noise is of thermal noise type at temperature below 448 K. Above 448 K, the detector shows a very different noise characteristic, i.e., the noise spectral density is increased by one order of magnitude within the whole frequency range (up to 100 kHz). As shown in Fig. 4(b), the calculated thermal noise based on the measured detector resistance and the temperature can be described as $i_{n,the} = \sqrt{4k_B TG}$. It is much lower than the measured total noise. Obviously, this enhanced noise is different from thermal noise. The observed noise at temperatures above 448 K is more like a flicker noise. The enhanced noise may be related to the gate leakage current and or the interface states in the AlGaN/GaN heterostructure. It has to be noted that the detector sensitivity can be recovered by lowering the temperature from 473 K to 300 K, i.e., no damage is made by heating the detec-

tor in air up to 473 K. However, at this moment the origin of this excess noise is not yet clear. To figure out the origin, more experiments are required in the future.

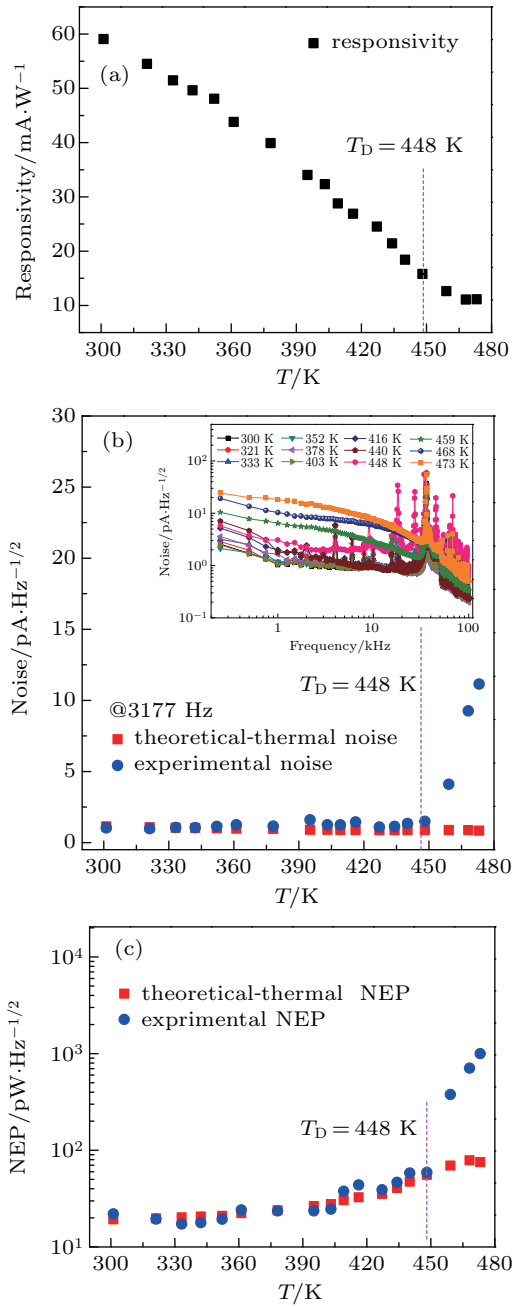


Fig. 4. (a) Maximum responsivity measured as a function of elevated temperature. (b) Noise spectra at elevated temperatures under an optimal gate voltage. (c) The experimental and theoretical noise equivalent powers of terahertz detector as a function of temperature from 300 K to 473 K.

Nevertheless, a demarcation temperature $T_D = 448$ K can be identified above which the detector behaves in an abnormal state. Below this temperature, the noise is relatively constant on the order of 1–2 pA/Hz$^{1/2}$ while the responsivity decreases linearly with temperature due to the falling of the conductance. As a result, the measured NEP as shown in Fig. 4(c) increases from 22 pW/Hz$^{1/2}$ to 60 pW/Hz$^{1/2}$ when the temperature is tuned from 300 K to 448 K. Hence, the increase in NEP by a factor of 2.7 is mainly caused by the decrease in responsivity from 300 K to 448 K. Moreover, with the increase of temperature from 300 K to 448 K, the electron mobility decreases by a factor of 2.9 from 1748 cm^2/V · s to 597 cm^2/V · s. The conclusion can be drawn that the decrease in the sensitivity of the detector is due to the reduction of electron mobility in the channel.

NEPs at different temperatures are calculated based on the theoretical thermal noise and compared with the measured values, as shown in Fig. 4(c). Good agreement can be seen at temperatures below 448 K. Above 448 K, the measured NEP increases sharply owing to the increased unknown noise but not the responsivity.

4. Conclusion

The dependences of responsivity and noise characteristic of AlGaN/GaN HEMT detectors on temperature have been studied by varying the temperature between 300 K and 473 K. The detector survives after four full thermal cycles. AlGaN/GaN-HEMT terahertz detectors are promising for applications at high ambient temperatures. A demarcation temperature around 448 K is identified. Below this temperature, the detector can be reliably operated and the sensitivity is limited by the thermal noise about 1–2 pA/Hz$^{1/2}$. When the temperature is tuned from 300 K to 448 K, the decrease in the detector sensitivity by a factor of three is due to a reduction of electron mobility in channel. When the detector temperature crosses the demarcation temperature, the noise shows an abrupt change from thermal-noise type into flicker-noise type. Further experiments would be required to uncover the origin of the observed strongly-enhanced noise at temperature above 448 K.

References

[1] Kleine-Ostmann T and Nagatsuma T 2011 *Journal Infrared, Millimeter, and Terahertz Waves* **32** 143
[2] Siegel P H 2004 *Microwave Symposium Digest, IEEE MTT-S International* **3** 1575
[3] Falconer R J and Markelz A G 2012 *J. Infrared Millimeterand THz Waves* **33** 973
[4] Dhillon S S, Vitiello M S, Linfield E H, *et al.* 2017 *J. Phys. D: Appl. Phys.* **50** 04300101
[5] Son J H 2009 *J. Appl. Phys.* **105** 1020331
[6] Echternach P M, Stone K J, Bradford C M, Day P K and Wilson D K 2013 *Appl. Phys. Lett.* **103** 053510
[7] Levinshtein M E, Rumyantsev R L, Gaska R, Yang J W and Shur M S 1998 *Appl. Phys. Lett.* **73** 1089
[8] Balandin A, Cai S, Li R, Wang K L, Rao V R and Viswanathan C R 1998 *IEEE Electron Device Lett.* **19** 475
[9] Levinshtein M E, Rumyantsev S L, Gaska R, Yang J W and Shur M S 1998 *Appl. Phys. Lett.* **73** 1089
[10] Sakong S H, Lee S H, Rim T, Jo Y W, Lee J H and Jeong Y H 2015 *IEEE Electron Device Lett.* **36** 229
[11] Hou H W, Liu Z, Teng J H, Palacios T and Chua S J 2017 *Sci. Rep.* **7** 46664

[12] Qin H, Li X, Sun J D, Zhang Z P, Sun Y F, Yu Y, Li X X and Luo M C 2017 *Appl. Phys. Lett.* **110** 171109
[13] Hou H W, Liu Z H, Teng J H, Palacios T and Chua S J 2017 *Appl. Phys. Express.* **10** 014101
[14] Sun J D, Sun Y F, Wu D M, Cai Y, Qin H and Zhang B S 2012 *Appl. Phys. Lett.* **100** 013506
[15] Yang X X, Sun J D, Qin H, Lv L, Su L N, Yan B, Li X X, Zhang Z P and Fang J Y 2015 *Chin. Phys. B* **24** 047206
[16] Li X, Sun J D, Zhang Z P, Popov V V and Qin H 2018 *Chin. Phys. B* **27** 068506
[17] Daumiller I, Kirchner C, Kamp M, Ebeling K J and Kohn E 1999 *IEEE Electron Device Lett.* **20** 448
[18] Abderrahmane A, Koide S, Okada H, Takahashi H, Sato S, Ohshima T and Sandhu A 2013 *Appl. Phys. Lett.* **102** 193510
[19] Daumiller I, Versan A, Heinle U, Scholz F and Kohn E 1997 *Proceedings of Advanced Concepts in High Speed Semiconductor Devices and Circuits*, August 4–6, 1997 Ithaca, NY, USA, p. 227
[20] Tan W S, Uren M J, Fry P W, Houston P A, Balmer R S and Martin T 2006 *Solid-state Electron.* **50** 511
[21] Knap W, Kachorovskii V, Deng V, Rumyantsev S, Lü J Q, Gaska R, Shur M S, Simin G, Hu X, AsifKhan M, Saylor C A and Brunel L C 2002 *J. Appl. Phys.* **91** 9346